Supporting information for:

Defect mitigation of Solution-Processed 2D WSe_2 Nano-flakes for Solar-to-Hydrogen Conversion

Xiaoyun Yu, Néstor Guijarro, Melissa Johnson, and Kevin Sivula*

Laboratory for Molecular Engineering of Optoelectronic Nanomaterials, École Polytechnique Fédérale de Lausanne (EPFL), Station 6, 1015 Lausanne, Switzerland
E-mail: kevin.sivula@epfl.ch

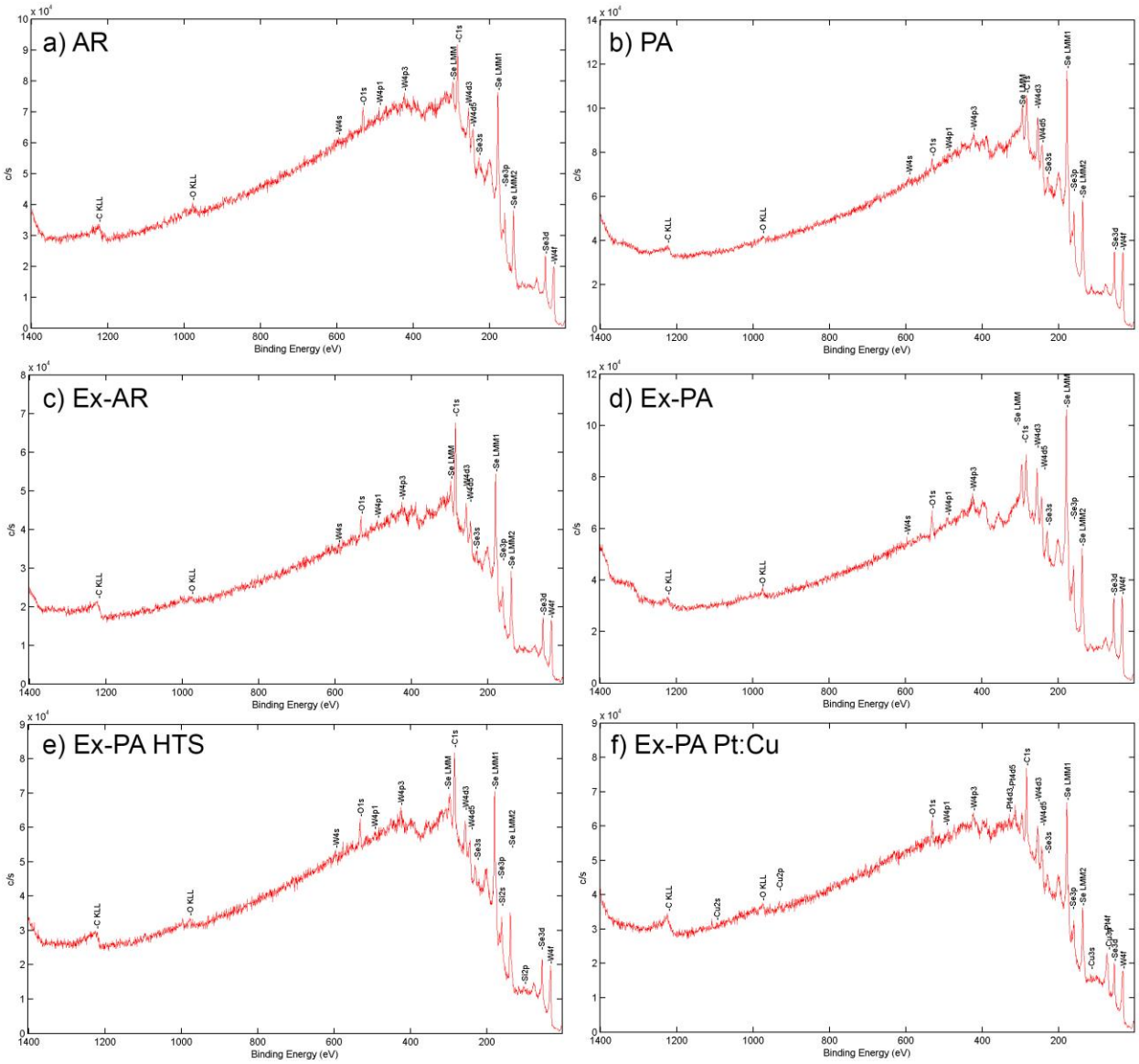

Figure S1. X-ray photoelectron spectroscopy (XPS) survey spectra of the as-received WSe_2 powder (a) and after pre-annealing (b). Scans were also performed after exfoliation (c) for the Ex-AR and (d) for Ex-PA samples, and after the HTS treatment (e), and after the deposition of the Pt:Cu catalysts and photoelectrochemical operation (f).

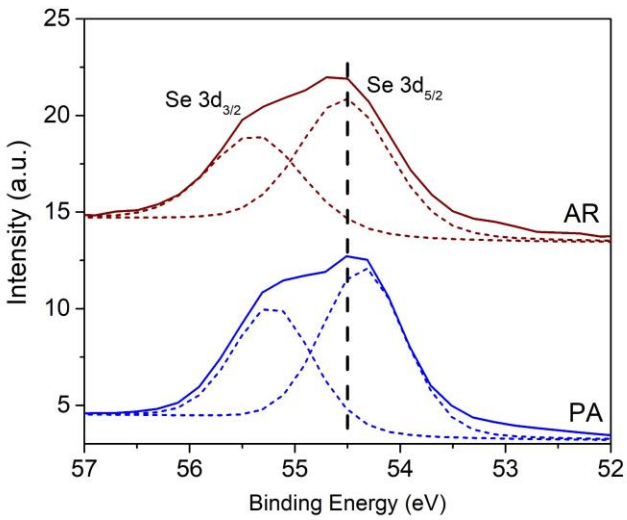

Figure S2. Detailed XPS spectra of the Se 3d region for both the AR (top) and PA (bottom) WSe_2 powders. The vertical broken line is indicated to show the shift of the peak to lower binding energy after the pre-annealing treatment.

Table S1. Estimated Se:W atomic ratios (uncalibrated) from XPS analysis of the WSe_2 under different conditions shows an increase in the Se:W ratio after the pre-annealing step.

	As-received WSe_2	Pre-annealed WSe_2
Powder sample	2.48	2.61[a]
After exfoliation	2.21	2.28

[a] may include elemental Se used in annealing step.

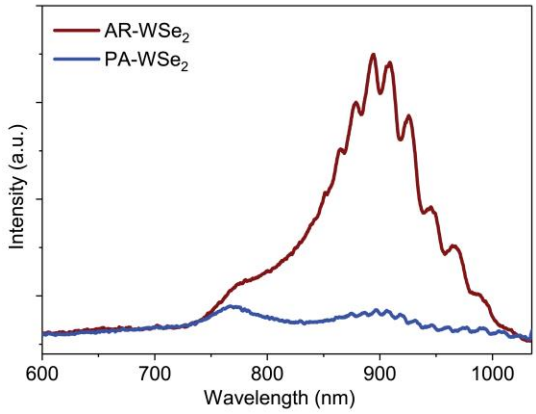

Figure S3. Room-temperature photoluminescence spectra of AR and PA WSe_2 (bulk) powders with a 532 nm excitation wavelength. The shoulder at 765 nm (1.62 eV) is ascribed to direct band exciton emission and a main peak at 900 nm (1.38 eV) due to excitons bound in deep traps, analogous to defect-induced PL signals observed for similar TMDs at room temperature.[1-2] Notably, this defect-induced PL signal is dramatically decreased after pre-annealing, implying a reduced trap density in the WSe_2. We note that a PL peak at around 1.4 eV (885 nm), which has been previously assigned to the phonon-assisted indirect band emission for few-atomic-layer WSe_2 sheets,[3] is not expected in the large bulk crystal powder examined here.[4]

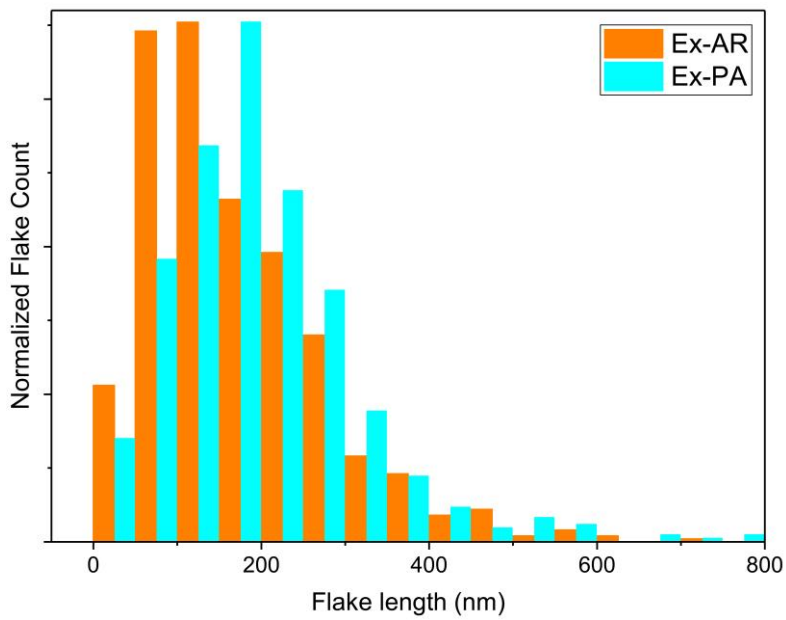

Figure S4. Normalized histograms of the lateral flake size (as estimated by TEM images of the deposited self-assembled WSe_2 films via image processing software) characterized by the long axis (as described in our previous work) in films prepared from exfoliated flakes of raw powder and the annealed powder.

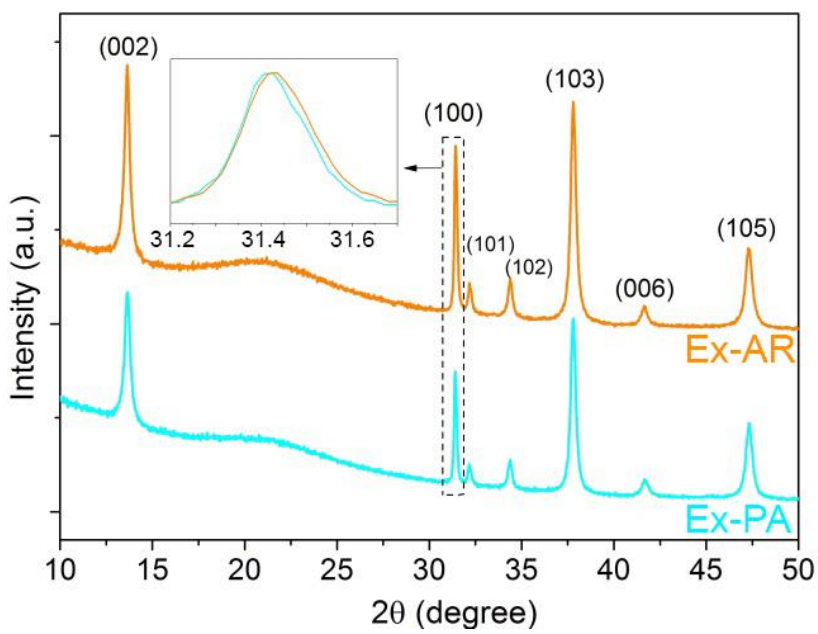

Figure S5. X-ray powder diffraction patterns of WSe_2 flakes exfoliated from as-purchased (orange line) and pre-healed (cyan line) WSe_2 bulk materials. Samples measured in 0.7 mm borosilicate capillaries. The detailed curves (inset) show narrower (100) peak for the healed-flakes compare to the raw-flakes. The average domain size in the basal plane can be estimated to be 76 nm for the raw flakes and 81 nm for the healed flakes.

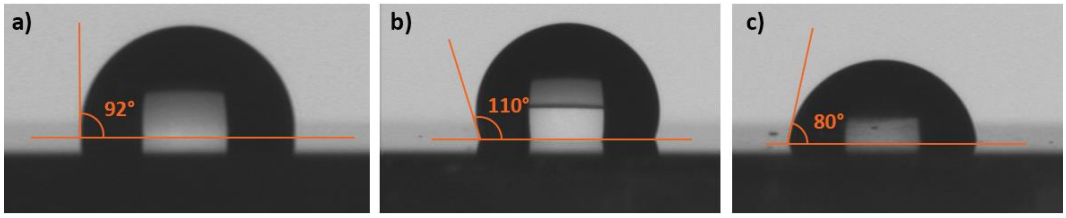

Figure S6. Water contact angle measured on the surface of an Ex-AR WSe_2 film (a), an Ex-AR-HTS film (b) electrode and a Ex-AR WSe_2 electrode treated with 1% 1,6-bis(trichlorosilyl)hexane toluene solution (c).

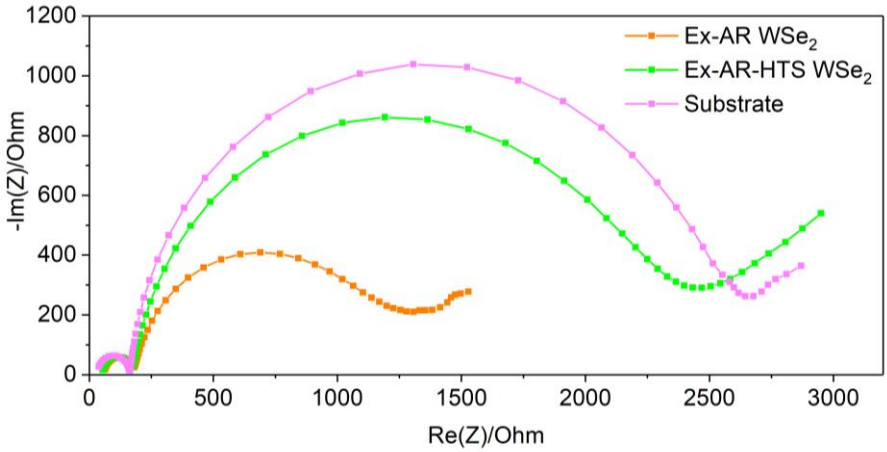

Figure S7. Electrochemical impedance spectroscopy (EIS) Nyquist plots for WSe_2 electrodes (with or without HTS treatment) and a blank (cPVPh/F:SnO_2) substrate measured in the dark in saturated Chloranil and 0.1 M NBu_4PF_6 electrolyte using acetonitrile as solvent at -0.2 V vs Ag/Ag+ applied potential. The charge transfer resistance was extracted from fitting the second semicircle.

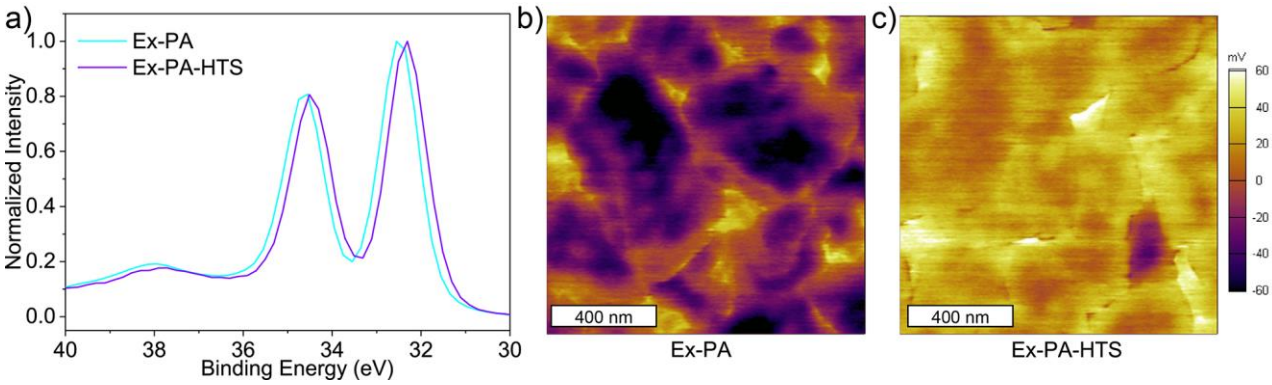

Figure S8. The surface potential effects of the HTS treatment are shown with (a) detailed XPS spectra of the W 4f region for both the EX-PA and Ex-PA-HTS WSe_2, and KPFM surface potential measurements of the Ex-PA (b) and (Ex-PA-HTS) self-assembled films on FTO.

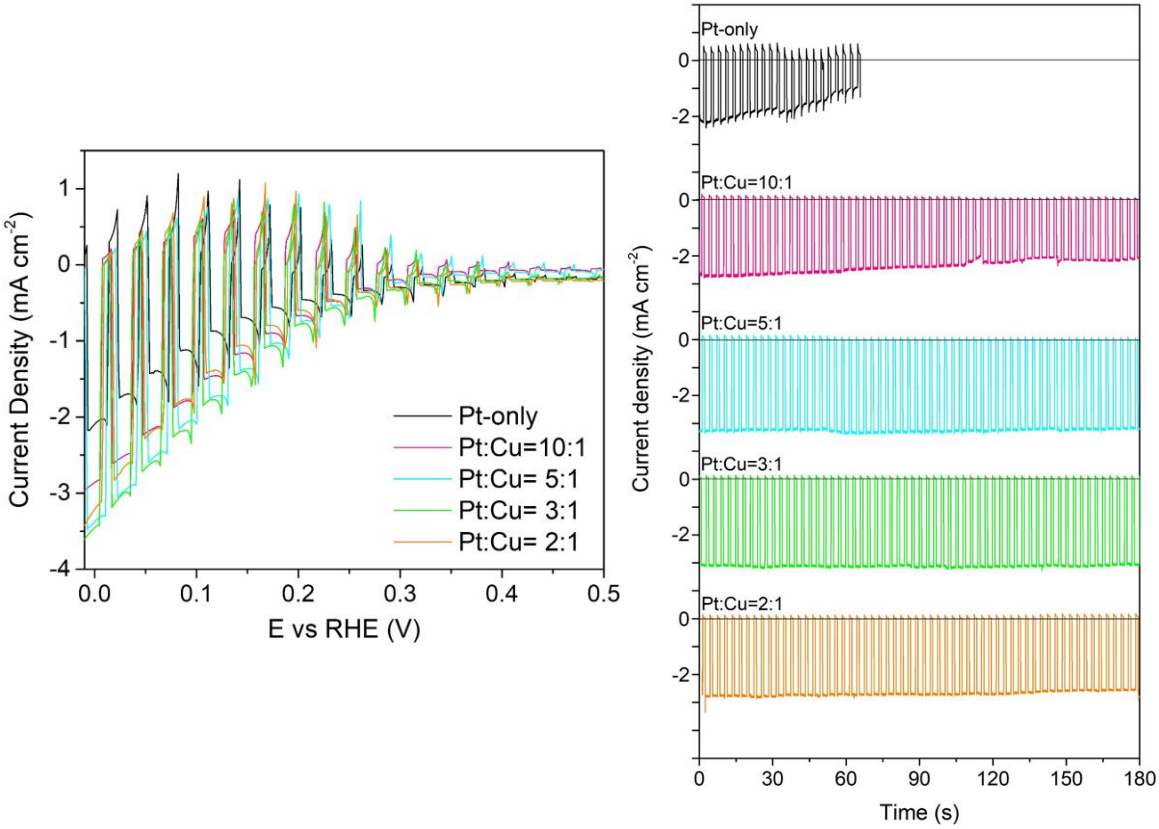

Figure S9. LSVs (left panel) and Chronoamperometric (right panel) stability (at 0 V vs RHE) of Ex-PA-HTS photocathodes after photodeposition (1.5 mC of total charge passed) of Pt:Cu co-catalyst with different feed ratios of Pt:Cu as indicated. Measured in 1 M H_2SO_4 at 0V vs RHE with vigorous Ar purging under intermittent (1 sun) illumination.

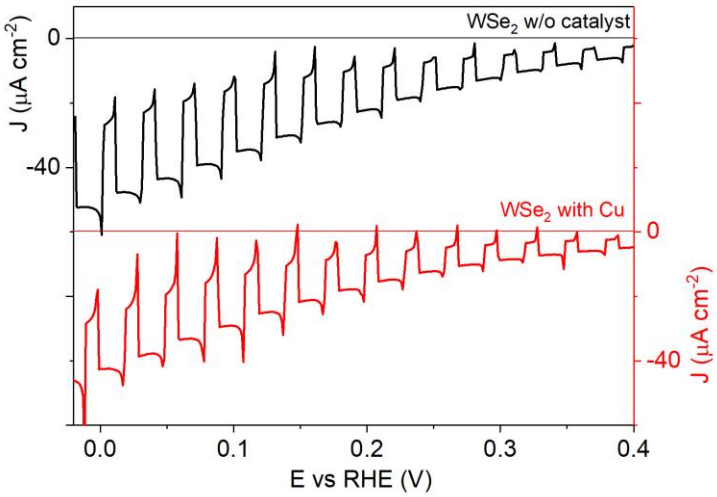

Figure S10. LSV curves for the WSe_2 Ex-AR electrodes before co-catalyst deposition (black) and after electrochemical deposition with only Cu precursors (tested in 1M H_2SO_4).

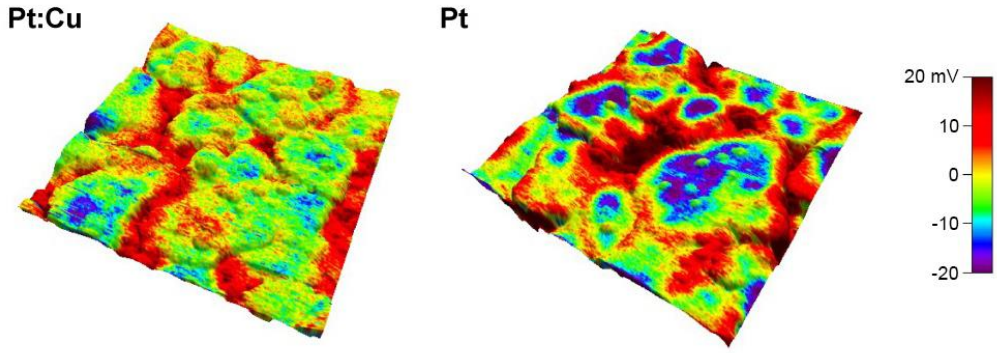

Figure S11. Kelvin probe force microscope (KPFM) results shown on 3D height structures present better surface potential homogeneity for WSe_2 flakes planar surface modified with Pt-Cu (left) than Pt (right) catalyst.

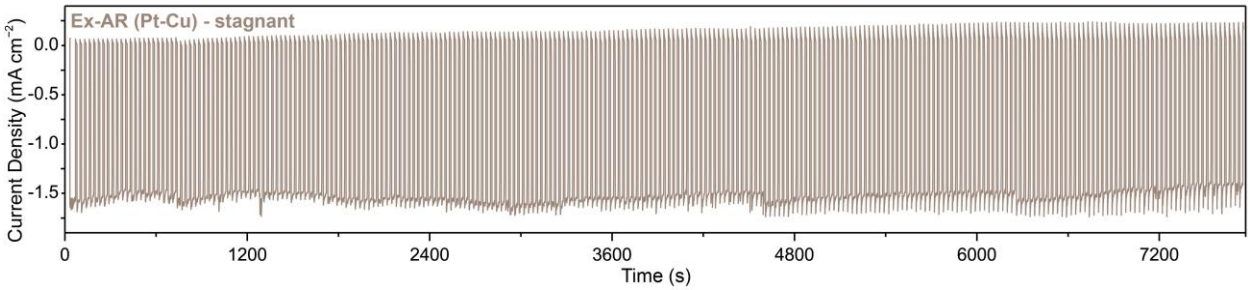

Figure S12. Chronoamperometric (CA) results (in 1 M H_2SO_4 at 0 V vs RHE) measured with in quiescent electrolyte of the Ex-AR WSe_2 photoelectrode with Pt-Cu co-catalyst under intermittent (1 sun) illumination.

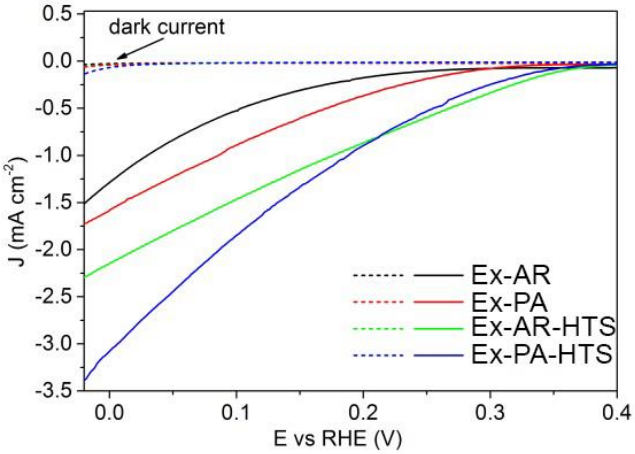

Figure S13. Linear scan voltammetry curves of WSe_2 electrodes measured in the dark (dashed curves) and under constant illumination (solid curves) in 1M H_2SO_4 electrolyte.

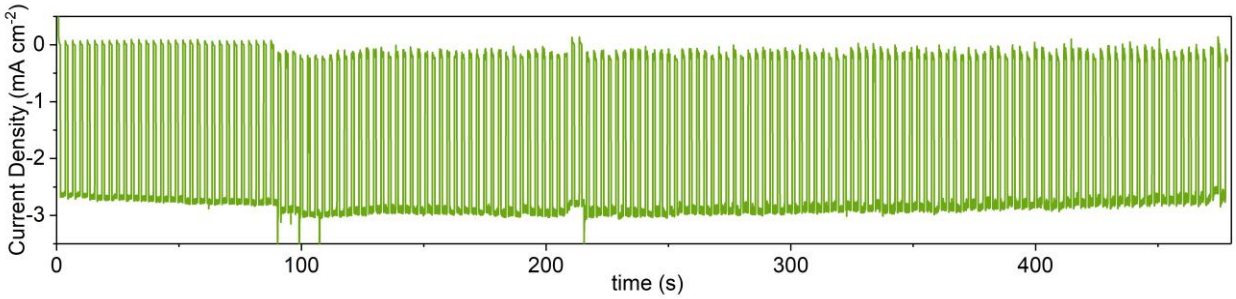

Figure S14. Chronoamperometric (CA) results (in 1 M H_2SO_4 at 0V vs RHE, measured with in electrolyte with vigorous Ar purging) of an HTS-treated WSe_2 photoelectrode (Ex-AR-HTS) with deposited Pt-Cu co-catalyst under intermittent (1 sun) illumination.

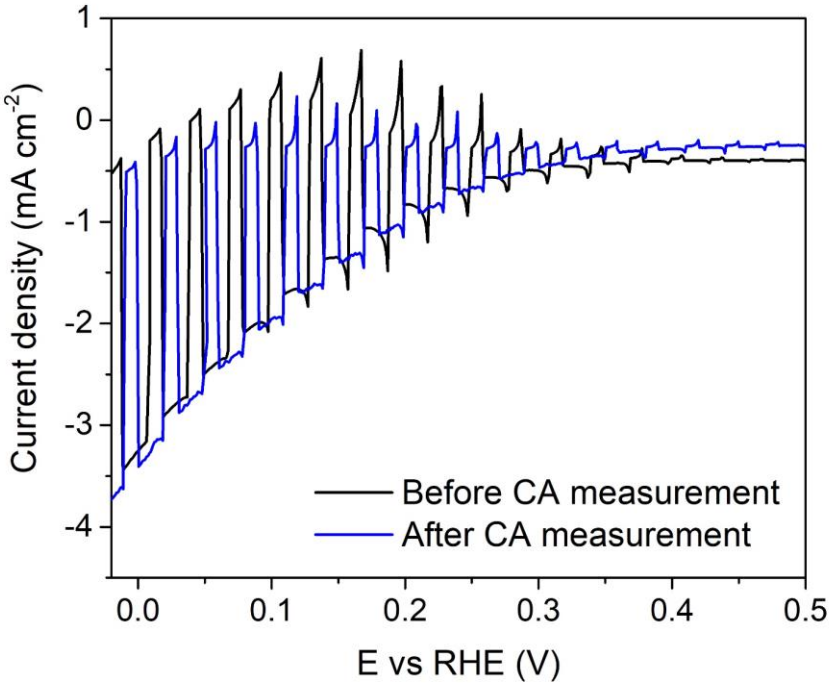

Figure S15. Linear scan voltammetry curves a Ex-PA-HTS Pt-Cu WSe_2 electrode after Pt:Cu deposition (before the chronoamperometry) and after CA measurement for 180 seconds in 1 M H_2SO_4 at 0V vs RHE, measured with in electrolyte with vigorous Ar purging under 1 sun illumination.

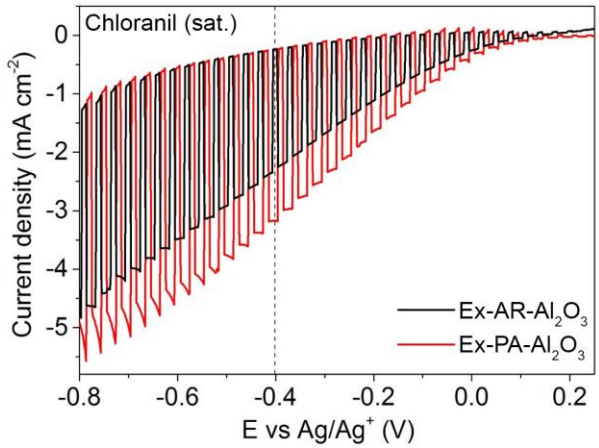

Figure S16. Linear scan voltammetry curves of WSe_2 electrodes treated with Al_2O_3 by ALD as previously reported[5] measured under intermittent illumination in saturated chloranil and 0.1 M NBu_4PF_6 electrolyte using acetonitrile as solvent. The dotted line represents the redox potential for the chloranil reduction reaction.

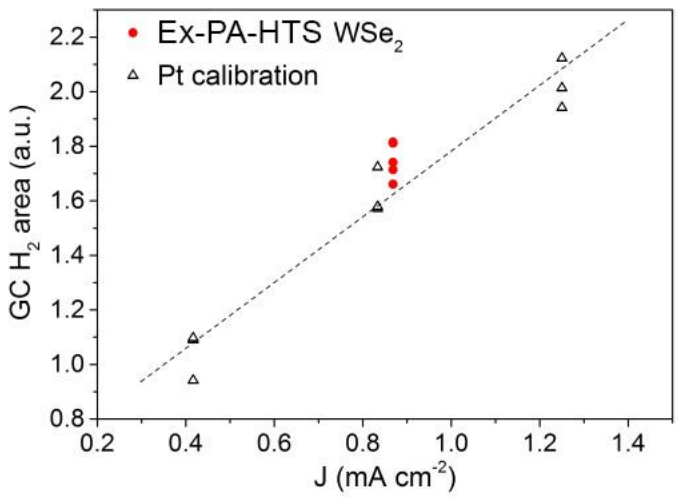

Figure S17. Measured H_2 peak area of GC response of either a control Pt electrode or an Ex-PA-HTS WSe_2 nano-flake electrode (active area of 0.236 cm^2) under Ar-purging in 1M H_2SO_4 electrolyte.

Supporting References.

(1) Chow, P. K.; Jacobs-Gedrim, R. B.; Gao, J.; Lu, T.-M.; Yu, B.; Terrones, H.; Koratkar, N., *ACS Nano* **2015,** *9*, 1520-1527.
(2) McCreary, A.; Berkdemir, A.; Wang, J.; Nguyen, M. A.; Elías, A. L.; Perea-López, N.; Fujisawa, K.; Kabius, B.; Carozo, V.; Cullen, D. A.; Mallouk, T. E.; Zhu, J.; Terrones, M., *J. Mater. Res.* **2016,** *31*, 931-944.
(3) Zhao, W.; Ghorannevis, Z.; Chu, L.; Toh, M.; Kloc, C.; Tan, P.-H.; Eda, G., *ACS Nano* **2012,** *7*, 791-797.
(4) Aruchamy, A., *Photoelectrochemistry and Photovoltaics of Layered Semiconductors*. Kluwer Academic Publishers: The Netherlands, **1992**.
(5) Yu, X.; Sivula, K., *Chem. Mater.* **2017,** *29*, 6863-6875.